Provided for non-commercial research and education use.
Not for reproduction, distribution or commercial use.

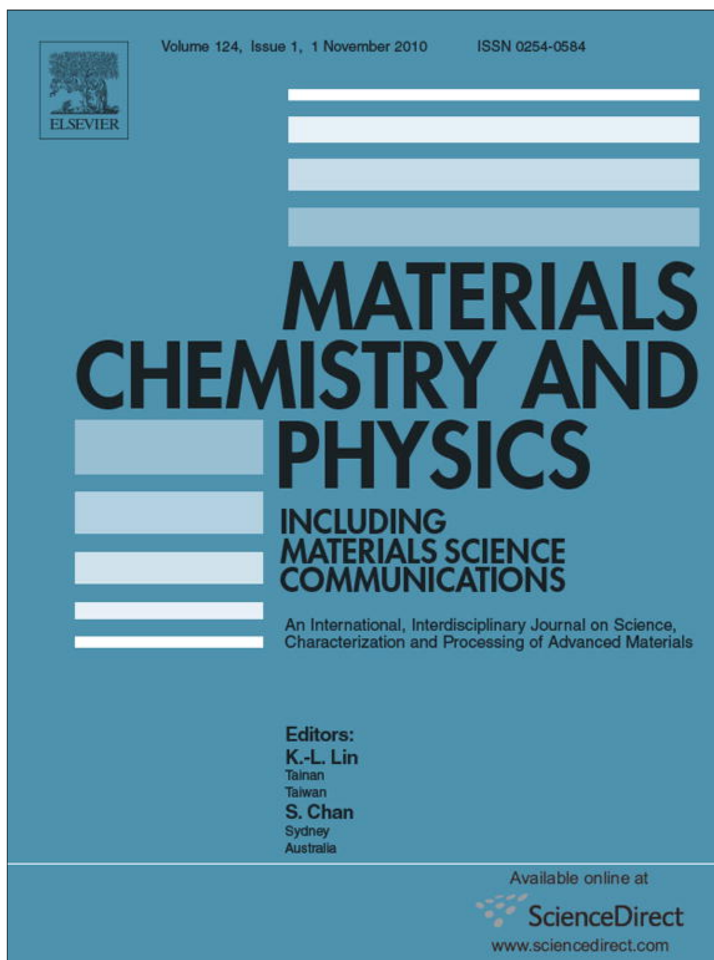

This article appeared in a journal published by Elsevier. The attached copy is furnished to the author for internal non-commercial research and education use, including for instruction at the authors institution and sharing with colleagues.

Other uses, including reproduction and distribution, or selling or licensing copies, or posting to personal, institutional or third party websites are prohibited.

In most cases authors are permitted to post their version of the article (e.g. in Word or Tex form) to their personal website or institutional repository. Authors requiring further information regarding Elsevier's archiving and manuscript policies are encouraged to visit:

http://www.elsevier.com/copyright

Author's personal copy

Materials Chemistry and Physics 124 (2010) 371–376

Contents lists available at ScienceDirect

Materials Chemistry and Physics

journal homepage: www.elsevier.com/locate/matchemphys

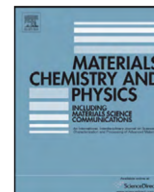

Copper viscoelasticity manifested in scratch recovery

Witold Brostow[a,*], Tea Datashvili[a], Robin McCarty[b], John B. White[b]

[a] Laboratory of Advanced Polymers & Optimized Materials (LAPOM), Department of Materials Science and Engineering and Department of Physics, University of North Texas, 1150 Union Circle # 305310, Denton, TX 76203-5017, USA
[b] Marlow Industries, Inc., 10451 Vista Park Road, Dallas, TX 75238-1645, USA

ARTICLE INFO

Article history:
Received 11 January 2010
Received in revised form 11 May 2010
Accepted 18 June 2010

Keywords:
Thermoelectric materials
Brittleness
Viscoelasticity
Scratch resistance

ABSTRACT

We have investigated two thick film copper compositions used in thermoelectric device fabrication. Dynamic mechanical analysis, thermal mechanical analysis, tensile testing, Vickers microhardness, optical microscopy and scratch testing were performed. The small grain samples have much smaller microindentation areas and much higher hardness than large grain samples, a consequence of intergranular spaces and thus low cohesion in large grain materials. The small grain material without intergranular spaces has higher linear thermal expansivity α_L up to 150 °C; above that temperature negative α_L is seen, a consequence of orientation relaxation. The large grain material also exhibits $\alpha_L < 0$ but only above 275 °C or so, a consequence of sintering. The small grain material has a storage modulus 49% higher than the large grain material over a wide temperature range, again an effect of high cohesion in the former. The brittleness value for the large grain material is 3.5 times larger than for the small grains material. Both kinds of materials exhibit recovery in scratch testing in the overall range of 23–36%—a manifestation of viscoelasticity.

© 2010 Elsevier B.V. All rights reserved.

1. Introduction and scope

Thermoelectric (TE) devices perform as heat pumps or heat engines where they experience large temperature differences (up to 250 °C) across the device [1]. A device is typically comprised of two ceramics that are metalized with copper, an array of TE elements, and solder bonding the device together as illustrated in Fig. 1. Because the device is comprised of many different materials, mechanical stress due to different isobaric expansivities (coefficients of thermal expansion) can translate stress to the brittle TE material. To ensure the long life of a TE device in operation, it is imperative to assess the stresses in the device and to alter designs to minimize this stress [2]. To properly model stresses in TE devices, material properties for all materials must be identified.

Characteristics of various TE materials have been reported before [3,4], including dynamic mechanical analysis (DMA) [5,6]. However, the material properties for the copper metallization, particularly when the copper metallization is produced using a screen printed thick film paste, are still unknown. Thick film copper metallization is made by screen printing fritted and/or fritless copper pastes on ceramic substrates and firing the paste at elevated temperatures in a controlled atmosphere furnace. Successive layers can be printed and fired to increase the thickness of the copper to the desired thickness—which can be up to 0.1 mm.

Steigerwald et al. [7] have reported how strongly the preparation procedure affects the structure and properties of copper. In this paper we report on the isobaric expansivity, DMA, tensile testing, Vickers microhardness, microindentation, optical microscopy, scratch resistance and sliding wear determination (evaluation of scratch resistance in service by multiple scratching along the same groove) of Cu samples prepared with fritted and fritless pastes.

2. Experimental

2.1. Materials preparation

Before firing, the unfritted copper paste, C1, consists of solvents and copper, while the fritted copper paste, C2, consists of solvents, copper oxide, copper, and glass. A mold with dimensions approximately 2.5 cm by 8.0 cm was made with adhesive tape, nominally 0.05 mm thick, on a smooth graphite block. For the unfritted paste, ten layers of tape were used to give a thickness of 0.5 mm, and for the fritted paste, five to seven layers of tape were used to give a thickness of 0.25–0.35 cm. The wet copper paste was then applied with a screen printing squeegee. The tape was removed leaving a rectangular pattern of wet paste. The wet paste was air dried for 75 min to remove some of the solvents prior to firing in an IR furnace. Typical temperatures for firing this copper paste are 900 to 950 °C. The unfritted copper paste results in a relatively uniform sample, but the unfritted paste results in a sample with large cracks. Smaller samples must be cut from the large one for testing.

* Corresponding author at: University of North Texas, Department of Materials Science and Engineering, 3940 North Elm. E 132, Denton, TX 76207, USA.
Tel.: +1 940 565 4358.
E-mail addresses: wbrostow@yahoo.com (W. Brostow), tcd0033@unt.edu (T. Datashvili), rmccarty@marlow.com (R. McCarty), JWHITE@marlow.com (J.B. White).

0254-0584/$ – see front matter © 2010 Elsevier B.V. All rights reserved.
doi:10.1016/j.matchemphys.2010.06.048

Author's personal copy

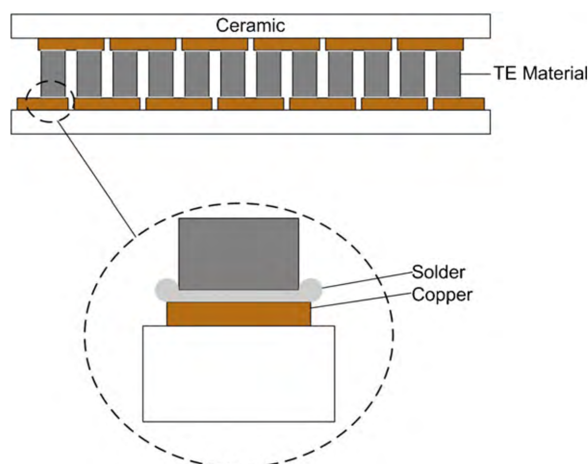

Fig. 1. Illustration of a typical TE device.

2.2. *Thermal mechanical analysis (TMA)*

The tests were carried out using a DMA7e apparatus from Perkin Elmer Co. Specimens were analyzed in rectangular form using a compression analysis kit in the temperature T scan mode. The experiments were performed over the temperature range from −50 to +300 °C at the heating rate of 10 °C min^{-1}.

TMA experiments provide values of linear isobaric expansivity (often called thermal expansion coefficient or CTE) defined as

$$\alpha_L = L^{-1}\left(\frac{\partial L}{\partial T}\right)_P \quad (1)$$

where L is the length (actually height, the distance between top and bottom parallel surfaces) of the sample, T is the temperature and P is the pressure. α_L has to be distinguished from volumetric isobaric expansivity $\alpha = V^{-1}(\partial V/\partial T)_P$ where V is the sample volume [8–10].

2.3. *Dynamic mechanical analysis (DMA)*

The DMA technique has been well described by Lucas et al. [11], by Gedde [12] and also by Menard [13,14]. We have used TA Instrument RSA3 DMA apparatus with a dual cantilever bending geometry. Dual cantilever fixtures clamp the ends of the specimen in place, introducing a shearing component to the distortion and increasing the stress required for a set displacement. The specimen is loaded with the clamps perpendicular to the long axis of the sample.

We have recorded the storage (solid-like) modulus E' and the loss (liquid-like) modulus E''. We also report values of $\tan\delta$ as a function of T, where

$$\tan\delta = \frac{E''}{E'} \quad (2)$$

The test parameters are listed in Table 1.

2.4. *Tensile testing*

The static tensile behavior of the samples was determined at room temperature with a MTS Model QTEST/5 machine. The tests were performed in a controlled environment and designed to determine the elongation at break, strain at break, and modulus. The cross-head speed was 50 mm min^{-1}; five specimens of each sample were tested, and average values are reported.

Table 1
DMA test conditions.

Parameters	Specifications
Initial static force	30.0 g
Auto tension sensitivity	2.0 g
Static > dynamic force by	50.0%
Minimum static force	2.0 g
Max. autotension displacement	3.0 mm
Max. autotension rate	0.01 mm s^{-1}
Max. applied strain	0.5%
Min. allowed force	2.0 g
Strain	0.03%

2.5. *Vickers microhardness*

The Vickers microhardness ($h_{Vickers}$) of each sample was determined using the dynamic microhardness measurement device, HMV-M Shimadzu Micro Hardness Tester Model M3 from Shimadzu Co., Kyoto, Japan.

Microindentations were made using a 300 g load. The holding time after completion of the indentation was 5 s. Five indentations were made for each sample. The mean value of the Vickers microhardness was calculated from five tests using the formula:

$$h_V = 1854.4\frac{P}{d^2} \quad (3)$$

Here P is the load in g while d is the mean diagonal of the indentation in μm. While the resulting value has dimensions, it is customary to list the Vickers microhardness as if it were a dimensionless quantity. We have used this technique before [15,16]; it is related to nanoindentation [17].

2.6. *Optical microscopy*

Surface images of the samples were taken using a Nikon Eclipse ME 600 microscope; the magnification was 10×.

2.7. *Scratch resistance*

We used a micro-scratch tester (MST) from CSM, Neuchatel, Switzerland. For each sample progressive scratch testing was performed. The parameters applied were: initial load 0.03 N, final load 5.0 N, loading rate 1.0 N min^{-1}, scanning load 0.03 N, scratch length 8.0 mm, scratch speed 1.6 mm min^{-1}, and room temperature. The conical diamond intender had a diameter of 200 μm and a cone angle of 120°. The scratch testing conditions were identical for all samples.

3. Microstructure and hardness

Optical microscopy was used to study surface microstructures in order to understand the microhardness behavior of the samples given the two different sample preparation procedures. Surface images of the samples were collected before and after indentations.

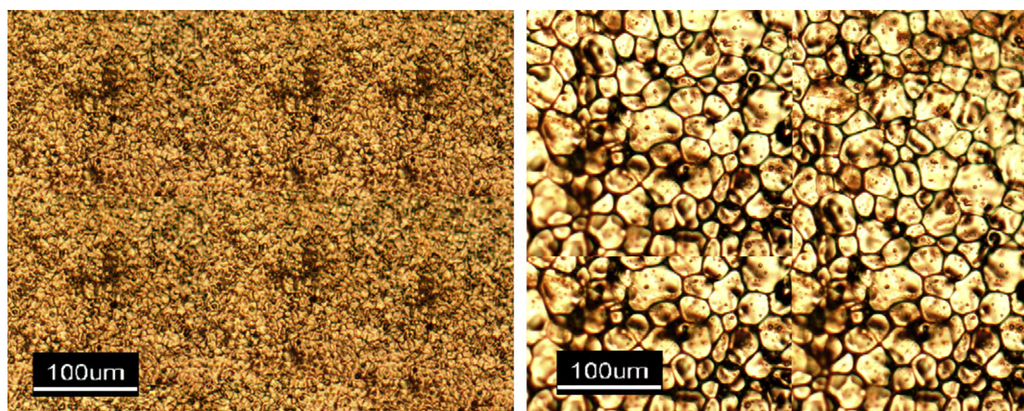

Fig. 2. (a and b) Micrographs of the C1 and C2 samples.

Author's personal copy

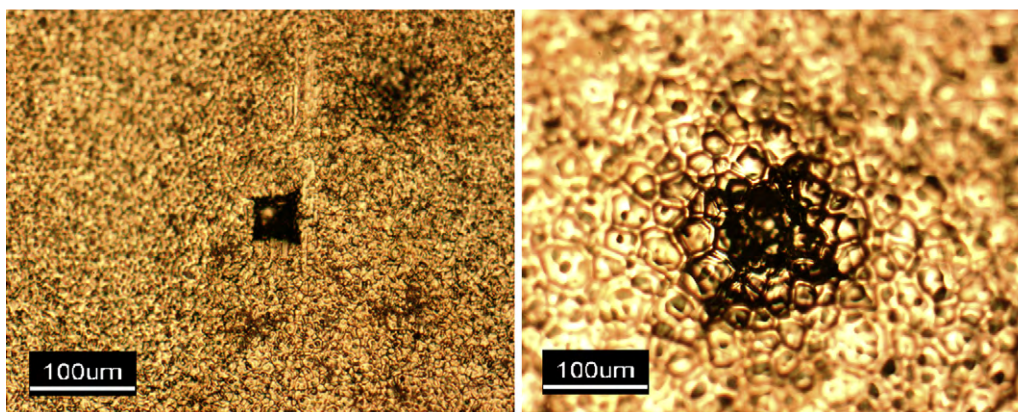

Fig. 3. (a and b) Micrographs of the C1 and C2 samples after indentation.

Fig. 2(a and b) represents the optical micrographs of the C1 and C2 samples.

We find clear differences. The optical image of the surface of the C1 sample shows relatively small grains with no cracks nor visible intergranular pores. By contrast, we see strikingly large intergranular spaces in the C2 sample. Kopczynska and Ehrenstein [18] discuss how interphases determine properties of materials that do not consist of a single continuous phase. Copper subjected to large deformations by Kommel et al. [19,20] undergoes significant structure changes. For Cu-containing alloys Wehr and Rylski [21] state: “It has been discovered that microstructure will critically affect interphase boundary formation, when copper is introduced into the Ag–Ni interfacial region. Copper mainly diffuses into nickel and less into silver.” Similarly, molybdenum impurities cause formation of fiber structures in copper [22] while titanium is used as a diffusion barrier and adhesion promoter for copper [7]. In our materials on a microscopic scale we see large grains in C2 compared with small grains in C1.

Fig. 3 shows the optical microscopy images after microindentation.

Dented area diagonals for C1 and C2 samples are 35.8 and 113.3 μm, respectively. Equivalent hardness values vary dramatically, they amount to 434.1 and 43.3. In C1 the indentation area is localized. In C2 the affected area is much larger than the area actually ‘attacked’ that has been in direct contact with the indenter.

Following the lines of Kommel et al. [19,20] and Wehr and Rylski [21], these results can be explained by microstructure and grain effects. Large intergrain areas in C2 deprive the material of cohesion and lower the capability to resist the stress exerted by the indenter. We see that the dented area diagonals and Vickers microhardness values both support this conclusion.

4. Thermal expansivity and dynamic mechanical properties

Fig. 4 shows TMA results for our samples for the temperature range from −50 to 300 °C.

In the temperature range from −50 to +150 °C both samples show an increase in dimensions. The average values of α_L for this range are 14.4×10^{-6} and $11.7 \times 10^{-6}\,K^{-1}$ for C1 and C2, respectively. Thus, C1 has 23% higher expansivity than C2—as expected from our microstructure analysis. Miller et al. [23] discuss the basic mechanism of thermal expansion in crystals in terms of increased vibrational energy. Clearly only atoms are recipients of this energy, whereas the empty intergrain spaces in C2 are not affected.

Negative values of thermal expansivity are known in various classes of materials [23] including polymer liquid crystals (PLCs) [24]. Singh explains negative α values in PLCs by contraction along the draw or orientation direction—a previous processing effect [24].

Our materials also display negative α_L, starting at approximately 160 °C and above for C1 and at a much higher temperature ~275 °C for C2. The effect in C1 can be explained also by shrinking and relaxation of previously induced orientation. The fact that shrinkage in C2 begins to occur at a much higher temperature is indicative of a *sintering* process that reduces the volume of intergranular spaces.

Fig. 5 displays DMA results, namely the storage modulus E' and $\tan\delta$ diagrams as a function of temperature for C1 and C2.

While changes with temperature are seen, consider for simplicity average values of the storage modulus E' over the entire temperature range from −50 to +350 °C. C1 sample has $E' = 1.35 \times 10^{11}$ Pa in this range while C2 has $E' = 9.05 \times 10^{10}$ Pa. A major reason for the 49% higher E' value for C1 than that for C2 is the absence of cracks and the absence of large intergranular spaces in C1—in contrast to those seen in Fig. 2b for C2. Thus, the results of the different testing techniques reported above lead to joint conclusions about intergrain properties having the dominant effect.

5. Tensile behavior and brittleness

The literature is not very eloquent on the relationship between the dynamic storage modulus E' and the tensile modulus E, except for the repeated statement that the respective values should be close. The fundamental difference is that in standard tensile testing the material is stretched continuously while in DMA there is repetitive oscillatory loading. We recall the basic definition of E in terms of the engineering stress σ and the engineering strain ε in

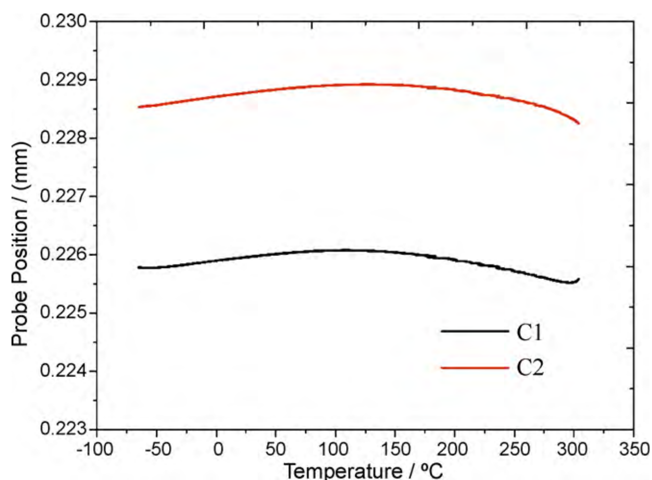

Fig. 4. TMA curves of the C1 and C2.

Author's personal copy

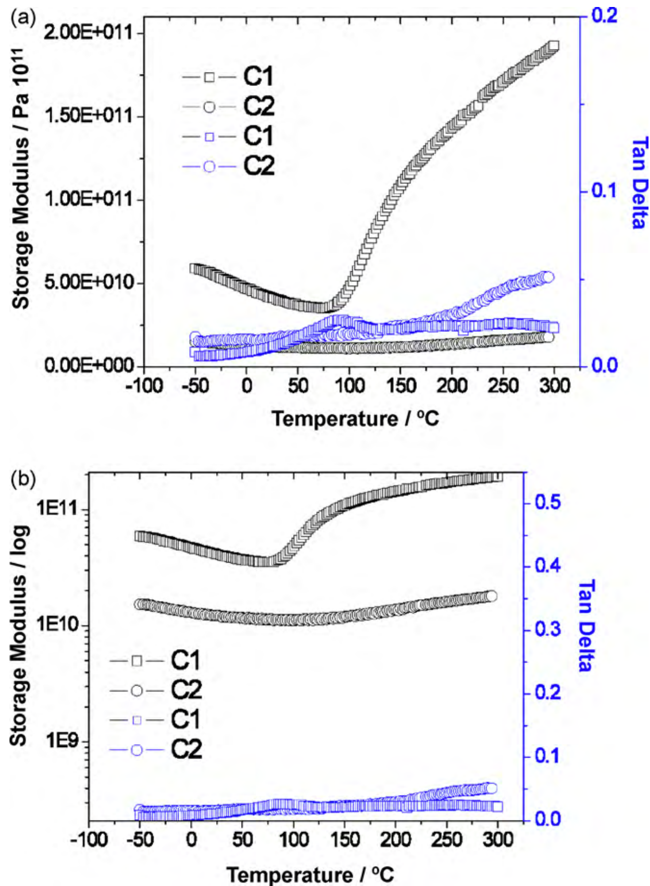

Fig. 5. DMA curves of the C1 and C2.

the linear elastic region:

$$E = \frac{\sigma}{\varepsilon} \quad (4)$$

In view of the definition, *if the sinusoidal loading remains within the elastic region*, we can expect close E and E' values. In contrast, for strongly deformed high density polyethylene we have found differences between E and E' because deformation causes discontinuities in the original undeformed structure [25]. As already discussed, our C2 sample preparation produces discontinuities. The tensile behavior of our specimens, materials significantly different from monocrystalline copper, is presented in Fig. 6 and summarized in Table 2.

As expected, the relative values between the two samples of the modulus and yield at stress obtained from stress–strain curves are in agreement with the DMA data. Young's modulus of the C1 sample is 1.9 times higher than that of the C2 material compared with E' that is 1.5 times higher. However, the actual measured values are considerably different, i.e. E' for C1 is 135 GP while E is 32 GP. Apparently continuing elongation shows weakness of the large grain material in a more significant way than sinusoidal loading.

Table 2
Thermal and mechanical properties.

Tensile property	C1	C2
Young's modulus E/GPa	32.1	16.6
Peak load/N	306.3	87.9
Peak stress/MPa	153.1	87.9
Strain at break/%	2.0	0.8
Stress at yield/MPa	11.3	7.2
Linear expansivity/°C	14.4×10^{-6}	11.7×10^{-6}

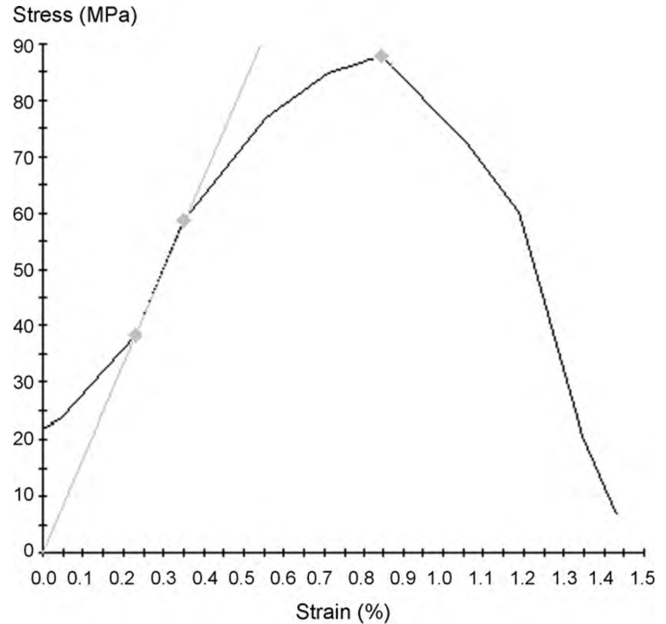

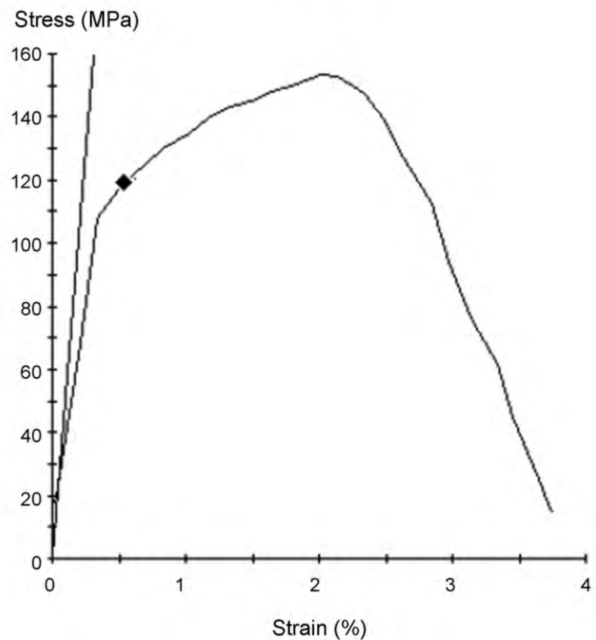

Fig. 6. Stress–strain diagrams of the C1 (a) and C2 (b).

We now return to the strain at break ε_b, which is an important parameter featured in the definition of material brittleness B [26] and used in a variety of applications [27,28]:

$$B = \frac{1}{(E'\varepsilon_b)} \quad (5)$$

Since our important objective is comparison of C1 with C2, we use E' for the entire temperature range from Section 3. From Eq. (5) we get $10^{10}\,B/(\%\text{Pa}) = 0.0368$ for C1 and 0.131 for C2 in the same units. Thus, brittleness values show the difference between C1 and C2 more dramatically than some other quantities; the ratio of B values is $\approx$3.5.

Author's personal copy

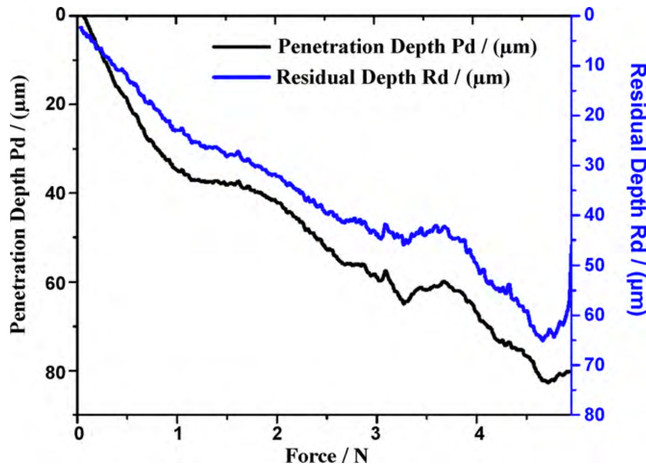

Fig. 7. Penetration depth R_p and residual depth R_h of the C1.

6. Scratch resistance

We have determined micro-scratch resistance of our materials since it is related to brittleness [26] and also to wear as described below. While not an important factor for TE devices, Rabinowicz [29] points out that wear is a source of large financial losses to other industries every year. In a different area, Gutmanas and Gotman [30] discuss importance of wear in human body replacement parts and also ways of minimizing wear in implants. For TE coolers or heaters, fatigue observed in DMA is more important; however, for completeness of evaluation we have obtained these more comprehensive characteristics of our materials.

Three parameters are relevant in scratch resistance determination: (i) maximum or instantaneous penetration depth R_p; (ii) residual or healing depth R_h (after 2 min); (iii) percentage viscoelastic recovery φ defined [31–33] as

$$\varphi\frac{R_p - R_h}{R_h} \cdot 100\% \qquad (6)$$

The definition (6) is usable in single scratching [31,33] as well as in sliding wear determination (SWD), that is multiple scratching along the same groove [34].

In each run made at a progressive force, we obtain the depth as a function of load. Results are presented in Figs. 7 and 8, respectively, for C1 and C2.

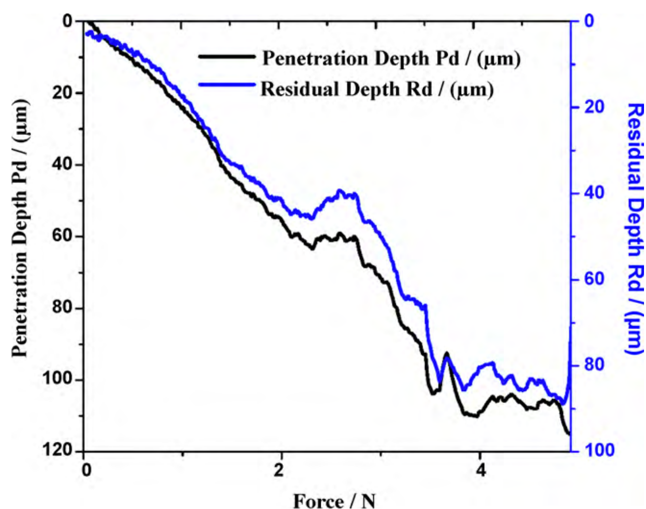

Fig. 8. Penetration depth R_p and residual depth R_h of the C2.

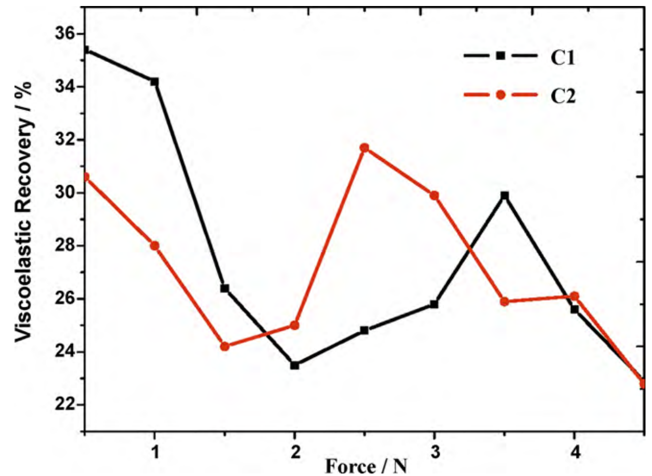

Fig. 9. Viscoelastic recovery of the samples.

It is clearly seen in Fig. 7 that C1 is more resistant to instantaneous deformation by micro-scratching. The original penetration depths R_p values of the C1 sample are changing from 0 to 80 μm in 0.03 to 5.0 N progressive force range, while the C2 material R_p values are changing from 0 to 120 μm. The situation is the same for the residual depth R_h; namely the C2 sample has relatively higher residual depth than the C1.

In Fig. 9 we can see the values of viscoelastic recovery as defined by Eq. (6)—also as a function of the force.

Changes of ϕ with load are a manifestation of surface inhomogeneity**.** The viscoelastic recovery of the C1 is changing from 23% to 36% while that of C2 is between 23% and 31%.

Once again microstructure differences and effects of grain boundaries manifest themselves.

7. Concluding remarks

While ϕ values for viscoelastic polymer-based materials are much higher such as 60–80% [32], the viscoelastic behavior of copper samples C1 and C2 is unmistakeable. Santosham and Ramsey [35] might have been the first ones who pointed out that copper, aluminum and mild steel exhibit signs of viscoelasticity. Kommel reported viscoelastic behavior of single crystal Ni-based superalloys [36]. There are some reports of viscoelasticity in Cu-containing composites such as Cu + an elastomer [37], but assigning viscoelastic behavior to the metal alone is difficult in such cases. These reports [37–39] are based on *mechanical* properties. *Tribological* properties are investigated much less than mechanical ones by far; the present paper might be the first one reporting manifestations of viscoelasticity in tribology for a metal.

Viscoelasticity is investigated most often by DMA [11–14]. DMA is also the technique of choice for locating glass transitions [38]. To conclude, let us mention some orders of magnitude involved. For low frequencies such as 1 Hz, materials with large viscoelastic effects at ambient temperatures, e.g. certain polymers, have loss tangent tan δ in the range 0.1–3. Glassy and crystalline polymers have values around 0.1. Soft cross-linked polymers have values such as 0.05 at 1 Hz [39]. Structural metals such as steel, brass, and aluminum have values of 10^{-3} or less, indicating small viscoelastic effects. For example and as discussed before [5], aluminum alloy type 6061-T6 has tan $\delta = 3.6 \times 10^{-6}$. Bismuth telluride tan δ values [5,6] are somewhere in between structural metals and viscoelastic polymers; the behavior of bismuth telluride might be explained in terms of movements along the van der Waals planes. Our copper samples have tan δ values in the range from 0.02 to 0.03.

Author's personal copy

Acknowledgments

Final stages of this project have been supported by the II-VI Foundation, Bridgeville, PA. Discussions with Kevin P. Menard are appreciated.

References

[1] H.J. Goldsmid, Electronic Refrigeration, Pion, London, 1986.
[2] R. McCarty, ANSYS Adv. 2 (2008) 26.
[3] H.L. Ni, T.J. Zhu, X.B. Zhao, Physica B 364 (2005) 50.
[4] J.E. Rodríguez, J. López, Physica B 387 (2007) 143.
[5] W. Brostow, K.P. Menard, J. White, Mater. Res. Soc. Symp. 691 (2002) G9.4.
[6] W. Brostow, K.P. Menard, J. White, e-Polymers no. 045 (2004).
[7] J.M. Steigerwald, S.P. Murarka, R.J. Gutman, D.J. Duquette, Mater. Chem. Phys. 41 (1995) 217.
[8] W. Brostow, V.M. Castaño, G. Martinez-Barrera, J-.M. Saiter, Physica B 334 (2003) 436.
[9] W. Brostow, V.M. Castaño, G. Martinez-Barrera, D. Pietkiewicz, Physica B 344 (2004) 206.
[10] G. Broza, V.M. Castaño, G. Martinez-Barrera, K.P. Menard, C. Simões, Physica B 357 (2005) 500.
[11] E.F. Lucas, B.G. Soares, E. Monteiro, Caracterização de Polímeros, e-papers, Rio de Janeiro, 2001.
[12] U.W. Gedde, Polymer Physics, Kluver, Dordrecht, 2001.
[13] K.P. Menard, in: W. Brostow (Ed.), Performance of Plastics, Hanser, Munich–Cincinnati, 2000 (Ch. 8).
[14] K.P. Menard, Dynamic Mechanical Analysis, 2nd ed., Taylor & Francis, Boca Raton, FL, 2008.
[15] W. Brostow, T. Datashvili, B. Huang, Polym. Eng. Sci. 48 (2008) 292.
[16] V.H. Orozco, W. Brostow, W. Chonkaew, B.L. Lopez, Macromol. Symp. 69 (2009) 277.
[17] B.D. Beake, G.A. Bell, W. Brostow, W. Chonkaew, Polym. Int. 56 (2007) 773.
[18] A. Kopczynska, G.W. Ehrenstein, J. Mater. Ed. 29 (2007) 325.
[19] L. Kommel, K. Kenk, R. Veinthal, Mater. Sci. Medziagotyra 8 (2002) 396.
[20] L. Kommel, A. Rozkina, I. Vlasieva, Mater. Sci. Medziagotyra 14 (2008) 206.
[21] A. Wehr, A. Rylski, J. Mater. Sci. 35 (2000) 777.
[22] A. Meskauskas, J. Dudonis, Mater. Sci. Medziagotyra 3 (1997) 9.
[23] W. Miller, C.W. Smith, D.S. Mackenzie, K.E. Evans, J. Mater. Sci. 44 (2009) 5441.
[24] R.P. Singh, in: W. Brostow (Ed.), Mechanical and Thermophysical Properties of Polymer Liquid Crystals, Chapman & Hall, London, 1998 (Ch. 10).
[25] Yu.M. Boiko, W. Brostow, A.Y. Goldman, A.C. Ramamurthy, Polymer 36 (1995) 1383.
[26] W. Brostow, H.E. Hagg Lobland, M. Narkis, J. Mater. Res. 21 (2006) 2422.
[27] W. Brostow, H.E. Hagg Lobland, Polym. Eng. Sci. 48 (2008) 1982.
[28] W. Brostow, H.E. Hagg Lobland, J. Mater. Sci. 46 (2010) 242.
[29] E. Rabinowicz, Friction and Wear of Materials, 2nd ed., Wiley, New York, 1995.
[30] E.Y. Gutmanas, I. Gotman, J. Mater. Sci. Med. 15 (2004) 327.
[31] W. Brostow, B. Bujard, P.E. Cassidy, H.E. Hagg, P.E. Montemartini, Mater. Res. Innovat. 6 (2002) 7.
[32] W. Brostow, J.-L. Deborde, M. Jaklewicz, P. Olszynski, J. Mater. Ed. 25 (2003) 119.
[33] W. Brostow, W. Chonkaew, L. Rapoport, Y. Soifer, A. Verdyan, J. Mater. Res. 22 (2007) 2483.
[34] B. Bilyeu, W. Brostow, L. Chudej, M. Estevez, H.E. Hagg Lobland, J.R. Rodriguez, S. Vargas, Mater. Res. Innovat. 11 (2007) 181.
[35] T.V. Santosham, H. Ramsey, Int. J. Mech. Sci. 11 (1969) 751–765.
[36] L. Kommel, Mater. Sci. Medziagotyra 15 (2009) 123–128.
[37] C.P. Chen, R.S. Lakes, J. Mater. Sci. 28 (1993) 4288–4298.
[38] W. Brostow, S. Deshpande, D. Pietkiewicz, S.R. Wisner, e-Polymers no. 109 (2009).
[39] W.H. Waddell, D.F. Rouckhout, M. Steurs, Kautschuk Gummi Kunststoffe 56 (2003) 525.